

Serveur Académique Lausannois SERVAL serval.unil.ch

Author Manuscript

Faculty of Biology and Medicine Publication

This paper has been peer-reviewed but does not include the final publisher proof-corrections or journal pagination.

Published in final edited form as:

Title: Characterization of Perfluorocarbon Relaxation Times and their Influence on the Optimization of Fluorine-19 MRI at 3 Tesla

Authors: E Darçot, R Colotti, D Brennan, GA Deuchar, C Santosh, RB van Heeswijk

Journal: NMR in Biomedicine

Year: 2019

Pages: e4212

DOI: 10.1002/nbm.4212

Accepted for publication in NMR in Biomedicine, October 2019

Title: A Characterization of ABL-101 as a Potential Tracer for Clinical Fluorine-19 MRI

Authors: Emeline Darçot, PhD¹, Roberto Colotti, PhD¹, David Brennan, PhD^{2,3}, Graeme A. Deuchar, PhD³, Celestine Santosh, MD^{2,3}, Ruud B. van Heeswijk, PhD^{1,4}

¹Department of Radiology, Lausanne University Hospital (CHUV) and University of Lausanne (UNIL), Lausanne, Switzerland

²Department of Neuroradiology, Institute of Neurological Sciences, Queen Elizabeth University Hospital, Glasgow, UK.

³Aurum Biosciences Ltd, Glasgow, UK.

⁴Center for Biomedical Imaging (CIBM), Lausanne and Geneva, Switzerland

Corresponding author:

Ruud B. van Heeswijk, PhD

Department of Radiology

Lausanne University Hospital (CHUV)

Rue du Bugnon 46, BH08.084

1011 Lausanne, Switzerland

Tel. +41-21-3147535

Ruud.MRI@gmail.com

Word count: 4383 words

Running Head: A Characterization of ABL-101 for Clinical Fluorine-19 MRI

Sponsors of the research, conflict of interest and source of funding: An ABL-101 sample was generously donated by Aurum Biosciences (Glasgow, UK). DB, GAD and CS received honoraria from the company Aurum Biosciences. RBvH has received grants from the Swiss National Science Foundation (SNSF, #PZ00P3_154719 and #32003B_182615). For the remaining authors none were declared.

List of abbreviations: BW, bandwidth; ETL, echo train length; f, frequency; LMR, longitudinal magnetization restoration; PFC, perfluorocarbon; PFD, perfluorodecalin; PFOB, perfluorooctyl bromide; PFPE, perfluoropolyether; ROI, region of interest; SD_{noise} , standard deviation of the background signal; SNR, signal-to-noise ratio.

Key words (up to 8): Fluorine-19 MRI; tracer; biocompatibility; detection limit; clearance half-life; perfluorocarbon.

Abstract

The two main challenges that prevent the translation of fluorine-19 (^{19}F) MRI for inflammation monitoring or cell tracking into clinical practice are 1) the relatively low signal-to-noise ratio generated by the injected perfluorocarbons (PFC), which necessitates long scan times, and 2) the need for regulatory approval and a high biocompatibility of PFCs that are also suitable for MRI. ABL-101, an emulsion of perfluoro(t-butylcyclohexane), is a third-generation PFC that is already used in clinical trials, but has not yet been used for ^{19}F MRI. The objective of this study was therefore to assess the performance of ABL-101 as a ^{19}F MRI tracer. At magnetic field strengths of 3, 9.4, and 14.1T, the CF_3 groups of ABL-101 generated a large well-separated singlet with T_2/T_1 ratios >0.27 , >0.14 and >0.05 , respectively. All relaxation times decreased with the increase of magnetic field strength. The detection limit of ABL-101 in a 0.25mm^3 voxel at 3T, 37°C and with a 3-minute acquisition time was 7.21mM . After intravenous injection, the clearance half-lives of the ABL-101 ^{19}F MR signal in mouse ($n=3$) spleen and liver were 6.85 ± 0.45 days and 3.20 ± 0.35 days, respectively. These results demonstrate that ABL-101 has ^{19}F MR characteristics that are similar to those of PFCs developed specifically for MRI, while it has clearance half-lives similar to PFCs that have previously been used in large doses in non-MRI clinical trials. Overall, ABL-101 is thus a very promising candidate tracer for future clinical trials that use ^{19}F MRI for cell tracking or the monitoring of inflammation.

Introduction

While fluorine-19 magnetic resonance imaging (^{19}F MRI) has existed for several decades,¹ it has seen a resurgence as a tool for inflammation monitoring and cell tracking in recent years.² Due to the lack of natural ^{19}F atoms in the human body, the received MR signal only originates from injected compounds, which makes the ^{19}F MR signal highly specific and directly proportional to the local concentration of the fluorine-containing compound. The most commonly used ^{19}F MR tracers are emulsions of perfluorocarbons (PFCs), chemically inert molecules that have previously been injected in large volumes (>0.5 L) in clinical trials in patients as blood volume expanders.³ After intravenous administration, PFCs are phagocytized by immune cells and predominantly removed from the circulation through exhalation and the reticuloendothelial system. Furthermore, given that PFCs are both lipophobic and hydrophobic,³ they rapidly clear from a tissue once the cell that carries them releases them or dies. Therefore, the change in their concentration (and thus ^{19}F MR signal) directly reflects changes in the concentration of the cells that were carrying them over time,⁴ which makes ^{19}F MRI a unique non-invasive monitoring tool for inflammation imaging. For these reasons, ^{19}F MRI has already been used in pre-clinical studies for inflammation monitoring in diseases such as myocardial infarction,⁵ inflammatory bowel disease,⁶ myocarditis,⁷ cancer,⁸ atherosclerosis,⁹ and brain inflammation,¹⁰ while pre-clinical cell tracking has been demonstrated for both stem cells¹¹ and leukocytes.¹² In humans, to our best knowledge PFCs have only been imaged to locally track dendritic cells at the site of injection.¹³

There are two main challenges for the translation of ^{19}F MRI into clinical practice. The first challenge is the relatively low signal-to-noise ratio (SNR) of ^{19}F MRI: the low concentration (on the order of mM at best) of injected PFC in the targeted tissues generates a small signal compared to routine ^1H MRI. The need for a sufficiently high SNR therefore limits the usable pulse sequences and often necessitates signal averaging, which leads to long acquisition times. The second challenge is the need for PFCs with a good biocompatibility while also being suitable for ^{19}F MRI. While the former is being incrementally

addressed through the development of optimized hardware,¹⁰ pulse sequences¹⁴ and signal processing methods,¹⁵ the latter challenge usually requires a larger investment: bringing a new compound from initial proposal to regulatory approval requires a series of costly preclinical and clinical trials.

Several studies that envisaged the translation of ¹⁹F MRI to the clinic have therefore focused on emulsions of perfluorooctyl bromide (PFOB, also known as perflubron and Oxygent)¹⁶ and perfluorodecalin (PFD, used in Fluosol and Perftoran), since these have been used in previous clinical trials and have promising short clearance half-lives in the body. However, both PFOB and PFD have unfavorable MRI properties: since their ¹⁹F groups are not magnetically equivalent and result in multiple resonances, developments of MR pulse sequences are needed to either acquire the signal of all resonances in more time,¹⁷ or to acquire only a small part of the resonances at the cost of signal loss, all while avoiding complications from the signal of multiple resonances.¹⁸ Other studies have instead focused on molecules with favorable MRI properties, such as perfluoropolyether (PFPE, Celsense Inc, Pittsburgh, Pennsylvania, USA), of which the clearance half-life is unknown, or Perfecta,¹⁹ which has never been used in clinical trials.

An alternative might therefore be ABL-101 (previously known as Oxybyte), which is a third generation intravenous PFC emulsion that is currently being developed by Aurum Biosciences Ltd (Glasgow, United Kingdom) for combined diagnostic and therapeutic clinical application in acute ischemic stroke.^{20,21} ABL-101 consists of perfluoro(*t*-butylcyclohexane) molecules in a 60% w/v concentration in saline, with egg phospholipid as an emulsifier.²² Perfluoro(*t*-butylcyclohexane) consists of five magnetically inequivalent CF₂ groups and a CF group on a hexane ring as well as three magnetically equivalent CF₃ groups in the *tert*-butyl part (Figure 1a). Its molecular formula is C₁₀F₂₀ and it has a molar mass of 500.08g/mol. It was initially developed for oxygen delivery after traumatic brain injury (by Tenax Therapeutics Inc, Morrisville, NC, USA), and its capacity as an oxygen carrier was among others investigated in animal models of brain injury,^{20,23} and acute respiratory distress syndrome.²⁴ Its capacity to enhance microvascular blood flow was also investigated in an animal model of arterial gas embolism.²⁵ Moreover, ABL-101 has already been used

in several clinical trials (including a safety trial) on traumatic brain injury,^{26,27} while a trial on its use after stroke is ongoing.²⁸

Given the promising regulatory status and physiological aspects of ABL-101, the goal of this study was to characterize ABL-101 for its use as a ¹⁹F MRI tracer. More specifically, the relaxation times at various magnetic field strengths and temperatures as well as its detection limit and clearance from the mouse spleen and liver were determined and compared to those of other PFCs used for ¹⁹F MRI.

Methods

Phantom preparation

A sample of ABL-101 was graciously provided by Aurum Biosciences Ltd (Glasgow, United Kingdom), and was used to make phantoms for both MRI and NMR experiments. The ABL-101 emulsion was guaranteed to be stable over a four-year storage period with a specific gravity of 1.25 – 1.35 and an osmolality of 280 – 400 mOsm/kg as well as a particle diameter ≤ 600 nm for 90% of the particles and ≤ 300 nm for 50% of the particles. Undiluted ABL-101 had a PFC concentration of 1.20 M, or a ¹⁹F concentration of 24 M. An MRI phantom was constructed for the detection limit experiments, and consisted of five NMR tubes with different mixes of ABL-101 and agar gel (2% w/v in distilled water, Sigma Aldrich, St. Louis, Missouri, USA) to provide a wide range of ABL-101 concentrations: 300.0 mM, 149.8 mM, 75.0 mM, 37.2 mM and 0mM, from tube 1 to tube 5, respectively. The five tubes were embedded in a 50 ml tube with the agar solution and no ABL-101. Agar was chosen in order to create gel phantoms with a structure close to that of soft tissue, given that ABL-101 will mostly be taken up in inflammation sites of soft tissues and organs of the reticuloendothelial system.

Two NMR tubes were prepared for the relaxometry experiments, one with pure ABL-101 (1.20 M PFC), and one with a mix of ABL-101 and 2% w/v agar (0.300M PFC), the same as used in tube 1 of the MRI phantom.

Relaxometry

NMR spectra were acquired on a 9.4 T spectrometer (AV4 400 MHz, Bruker, Billerica, Massachusetts, USA) equipped with a broadband fluorine observe (BBFO) 5 mm probe, and on a 14.1 T spectrometer (AV3HD 600 MHz, Bruker) equipped with an N₂-cooled broadband observe (BBO) 5 mm cryoprobe. The chemical shift reference was trifluoroacetic acid (TFA). T₁ and T₂ relaxation times were measured at 24°C and 37°C in both NMR tubes, and both at the CF₃ resonance frequency (f) and four resonance frequencies that belong to the strongly J-coupled CF-CF₂ group of peaks (f = -115, -125, -138, -144 ppm). The T₁ relaxation times were obtained by acquiring a saturation recovery with 16 variable delays ($v_d = 0.001\text{-}5$ s) and applying an inverted exponential decay fit.

When possible, the T₂ relaxation times were obtained by acquiring a Carr-Purcell-Meiboom-Gill (CPMG) $n(\tau\text{-}\pi\text{-}\tau)$ echo train acquisition with $\tau = 10$ ms and with 16 variable counter increments ($n = 1\text{-}30$), and applying an exponential decay fit.

MRI was performed on a 3 T clinical MR scanner (MAGNETOM Prisma, Siemens Healthcare, Erlangen, Germany) with a 35-mm RF volume coil that is tunable to both ¹H and ¹⁹F frequencies (Rapid Biomedical, Rimpar, Germany).

The T₁ and T₂ relaxation times of the CF₃ resonance and the highest peak of the CF-CF₂ resonances were measured at 24°C and 37°C in both NMR tubes. The T₁ relaxation times were measured with an unlocalized inversion recovery spin echo with short adiabatic RF pulses (a hyperbolic secant inversion pulse with duration 4 ms, a 90° BIR-4 excitation pulse with duration 5.1 ms, and a hyperbolic tangent refocusing pulse with duration 4.1 ms), repetition time/echo time TR/TE = 10'000/10 ms, and 16 averages. Eight inversion times from 25 ms to 4000 ms were acquired. The same excitation and refocusing RF pulses were used in an unlocalized spin echo for the determination of the T₂ relaxation time of the highest peak of the CF-CF₂ resonances, with seven TE from 10 ms to 1000 ms. A CPMG multi-echo spin echo pulse sequence with two constant spoiler gradient pairs was used to map the T₂ relaxation time at the CF₃ frequency with the following parameters: TR = 7000 ms, echo spacing 30 ms, echo train length ETL = 32, pixel bandwidth

BW = 175 Hz/px, matrix size 128x128, slice thickness 20 mm, spatial resolution 1x1 mm², and total acquisition time 14min49 s. The first echo was not used since it lacks the minor contribution of stimulated echoes of the later points, and would skew the T₂ fit.²⁹ Image intensities were averaged for a large homogeneous region of interest in the vials, and T₂ values were calculated from a curve fit of these averaged intensities.

All relaxation times were expressed as relaxation time ± standard deviation that were obtained from the exponential fit calculation.

Pulse sequence optimization

For the TSE pulse sequence, Bloch equation simulations were performed in MATLAB (MathWorks, Natick, Massachusetts, USA) to generate maps of the signal per unit time as a function of TR, ETL and BW for the ABL-101 T₁ and T₂ relaxation times at 3 T, at both 24°C and 37°C, and for both the CF₃ resonance and the highest frequency of the CF-CF₂ multiplet. The optimized parameters were defined as those that enabled the maximum signal strength per unit time.^{14,30} The simulations were run with and without a longitudinal magnetization restoration (LMR) RF pulse of -90° after the echo train.

For the bSSFP pulse sequence, the optimal flip angle α was calculated as:³¹

$$\alpha = \arccos \frac{T_1/T_2 - 1}{T_1/T_2 + 1} \quad [1]$$

Detection limits

The lowest detectable concentration for a given scan time (i.e. the detection limit) of ABL-101 was determined with the five-tube phantom described above, at the CF₃ resonance frequency. The acquisition was performed with a 3D TSE pulse sequence with the LMR off and on, as well as with the bSSFP pulse sequence. For the abovementioned TSE pulse sequence, the excitation and refocusing RF pulses were modified sinc pulses with durations of 3.84ms and 5.12ms, and bandwidths of 1360Hz and 680Hz, respectively. The optimized TR and ETL, as well as the following parameters were used: matrix size = 128x64, 32 slices, spatial resolution = 0.5x0.5x1 mm³. The bSSFP pulse sequence was used with the

optimized flip angle, TE/TR = 5.17ms/10.3ms, matrix size = 128x128, 32 slices, and spatial resolution = 0.5x0.5x1 mm³. The SNR was measured for each tube as the ratio between the average of the signal intensity of the segmented tube and the standard deviation of the background signal (SD_{noise}), selected as a large region of interest (ROI) outside the phantom. A linear fit was then made with SNR as function of the ABL-101 concentration. The detection limit was defined as the Rose criterion,³² i.e. the concentration at which the SNR = 4.

The common animal anesthetic isoflurane might generate a confounding signal in ¹⁹F MR images when ABL-101 is used, and thus reduce the specificity of ¹⁹F MRI.^{33,34} To test this, a syringe with pure ABL-101 and a syringe with pure isoflurane were imaged together with the abovementioned TSE pulse sequence; once with the transmitter frequency set to the closest isoflurane resonance, and once set to the ABL-101 CF₃ resonance.

Biological half-life

A longitudinal study was performed on C56Bl/6 male mice (n=3, Charles River Laboratories, L'Arbresle, France). Permission from the local Animal Ethics Committee was obtained for all animal experiments performed in this study. Tail vein injections of ABL-101 were performed with a dosage of 3 ml/kg body weight, which is equivalent to the highest dose administered in clinical trials using this PFC emulsion.²⁶⁻²⁸ The injection volume was 73±5 µl of ABL-101 (for a mouse weight 24.6±1.4 g).

The mice were scanned once a week, starting at day 1 after injection. In compliance with the ethics protocol, no further scan sessions would be scheduled after week four if the ¹⁹F signal intensity was lower than half the ¹⁹F signal measured at week one.

The imaging protocol was as follows: a ¹H 3D gradient-recalled echo (GRE) pulse sequence was used for anatomical localization, with TR/TE = 50/3.18 ms, flip angle = 40°, BW = 270 Hz/px, matrix size = 64x64, number of slices = 32, isotropic spatial resolution = 1 mm³. For ¹⁹F MRI, a 3D TSE pulse sequence was acquired with the same RF pulses as mentioned above and with the parameters defined for the CF₃ frequency at 37°C (TR/TE = 2900/13 ms, ETL = 32 and BW = 130 Hz/px), matrix size = 64 x 64, slices =

32, isotropic spatial resolution = 1 mm³, number of averages = 6, and a total acquisition time = 20 min 50 s.

Anesthesia was induced with 3% isoflurane in oxygen for ~2 minutes and then reduced to 1.5-2% isoflurane for the duration of the scan. A tubing system with circulating hot water placed on top of the mouse body was used to maintain the mouse temperature at 37±0.5°C. The mouse temperature and respiration were monitored with a rectal probe and a respiration pillow placed beneath the mouse abdomen, respectively (SA Instruments, Stony Brook, New York, USA).

Images were reconstructed from raw data with MATLAB. The threshold of the ¹⁹F images was set at 4×SD_{noise}, which removed 97% of the background noise signal. Interpolation and co-registration of the ¹⁹F images to ¹H images was performed to allow the ¹H/¹⁹F overlay for visualization purposes. Segmentation of the spleen and liver was performed after thresholding on the unprocessed raw ¹⁹F images: high signal intensity ROIs were drawn through multiple slices in the spleen and liver. Published sizes and locations of the mouse spleen³⁵ and liver³⁶ were used as a ROI size reference. An exponential decay fit of the SNR measured in spleen and liver as a function of the acquisition dates was performed for each mouse with the following equation:

$$S(t) = S_0 \cdot \exp(-\lambda t), \quad [2]$$

where S is the SNR measured at time t, S₀ is the SNR at t=0 and λ is the reaction rate coefficient. The clearance half-life was then defined as $t_{1/2} = \frac{\ln(2)}{\lambda}$ and is expressed as average ± standard deviation of the individual clearance half-lives of the three mice used for the in vivo experiment for both the spleen and the liver.

Results

The ABL-101 spectrum consists of a main resonance (from the CF₃ groups) and a multiplet of smaller resonances that corresponds to the J-coupled CF and CF₂ groups at a distance of >50 ppm (Figure 1).

Relaxation times

The T_1 and T_2 relaxation times of ABL-101 both decreased with the increase of the magnetic field strength (Table 1). At both 9.4 T and 14.1 T and for both tested temperatures, when measured at the CF_3 resonance frequency, the pure ABL-101 consistently had a slightly lower T_1 relaxation time than the agar mix. While this behavior was observed as well for the T_2 relaxation time at 14.1 T, it was inverted at 9.4 T: the T_2 relaxation time of pure ABL-101 was slightly higher than that of the agar mix for both tested temperatures (Table 1). The T_1 and T_2 relaxation curves at both temperatures followed their models very well and could be fitted with high precision ($R^2 > 0.999$, Figure 2). The T_2/T_1 ratios of the CF_3 peak at 3 T in the ABL-101-agar-mix tube were similar at 0.31 and 0.27 at 24°C and 37°C respectively. The T_2/T_1 ratios in pure ABL-101 were at 0.39 and 0.29 at 24°C and 37°C, respectively. The T_1 relaxation time of the four investigated CF- CF_2 resonances varied from 804 ± 6 at 24°C to 1237 ± 10 ms at 37°C (Table 2). The T_2 relaxation times measured at 3 T for the largest resonance of the CF- CF_2 groups were on the order of 4-5 ms.

Optimized pulse sequence parameters

The relaxation times of the CF_3 resonance allowed for a broad optimum for the TSE pulse sequence, both without and with the LMR (Figure 3). While the temperature had a large influence on the parameters for both the CF_3 and CF- CF_2 resonances, the use of the LMR pulse only had an effect on the optimal parameters at the CF_3 frequency. At the CF_3 frequency at 3 T, the optimized flip angle for the bSSFP pulse sequence varied little, from 64° to 57°, respectively (Table 3), despite the variations in relaxation times between 24°C and 37°C.

Detection limits

The multi-compartment ABL-101 phantom resulted in homogeneous ^{19}F signals without any ghosting artifacts (Figure 4a). All linear regressions fitted the SNR measurements very well ($R^2 > 0.99$ for all, Figure 4b), and the ABL-101 detection limit of the three pulse sequences at both temperatures were all on the same order (Table 4).

In the scans with the isoflurane and ABL-101 vials, the closest isoflurane resonance had a frequency difference of 21ppm with that of ABL-101 (~2500Hz at 3T). When the transmitter frequency for the ^{19}F TSE was set to the resonance frequency of either of the compounds, only the vial with that compound was visible in the resulting image (Figure 5).

Biological half-life

^{19}F MR signal was observed in the spleen and liver of all mice at day 1 after injection. No effect of the injection on the mice was observed. The signal was cleared from the liver at day 15 already and remained visible in the spleen until the last measurement (Figure 6c-f). The size of the segmented spleen in the unprocessed ^{19}F images was $0.046 \pm 0.001 \text{ cm}^3$, and the size of the segmented liver was $0.79 \pm 0.17 \text{ cm}^3$.

The clearance half-life from the spleen and liver were 6.85 ± 0.45 days and 3.20 ± 0.35 days, respectively (Figure 6g).

Discussion

We successfully characterized the relaxation times, detection limits and biological half-life of the perfluorocarbon emulsion ABL-101 at several magnetic field strengths and temperatures in order to evaluate its potential as a tracer for fluorine-19 MRI.

In the MR spectrum, the 9 fluorine atoms of the CF_3 groups result in an uncoupled singlet with a chemical shift difference of >50 ppm from the CF-CF_2 multiplet. This allows for the use of routine pulse sequences at the CF_3 frequency without any ghosting artifacts from the CF-CF_2 multiplet with most excitation and refocusing bandwidths. Conversely, in this manner only 9/20 fluorine atoms in the perfluoro(t-butylcyclohexane) molecule are used for imaging, which leads to a lower total signal than if all 20 atoms would be excited. Similarly, only exciting the CF-CF_2 multiplet with an ultrashort-TE bSSFP pulse sequence³⁷ will only excite the other 11/20 atoms. The above-mentioned large chemical shift between the singlet and multiplet and the small chemical shifts between the individual CF-CF_2 resonances will make recently published pulse sequences that do acquire signal from multiple resonances^{17,38} quite challenging due to the required RF bandwidths.

On the one hand, when comparing the ABL-101 CF₃ singlet to other PFCs routinely used for ¹⁹F MRI, the 9 contributing atoms are fewer than the 20 of perfluoro-15-crown-5-ether (PFCE) and 48 of PFPE (Celsense). On the other hand, these emulsions tend to be prepared at lower ¹⁹F concentrations around 4 M³⁹ compared to the 24 M of ABL-101, meaning that higher effective doses of ABL-101 can be injected with an equivalent volume. Furthermore, when comparing the well-separated ABL-101 CF₃ singlet to singlets of PFCs that have been used in clinical trials, the 9 atoms generate more signal than the equivalent 3 and 4 atoms of PFOB and PFD, while the ¹⁹F concentration in the emulsion is similar at 20-24 M.⁴⁰

The T₂/T₁ ratio of ABL-101 compare in a similar manner to those of other PFCs that have a similar spectral profile. Interestingly at 9.4 T and 37°C the T₂/T₁ ratio of the ABL-101 CF₃ group was more similar to that of PFD, which does not have any CF₃ groups, than that of the CF₃ group of PFOB.⁴⁰ This might be caused by a combination of the different magnetic shielding of these groups, the size and structure of the various molecules, and the presence of the bromine atom in PFOB. At 3 T, the T₂/T₁ ratio was not as high as that of PFCE but was very close to those of PFOB and PFPE at 24°C and 37°C.³⁹ This indicates that the obtained SNR per unit of time and per ¹⁹F atom of the pulse sequences should be at least as good as that for PFOB or PFPE at 3 T. Both the T₁ and the T₂ relaxation times decreased with increasing magnetic field strength, although the T₂ values decreased more strongly, as also seen for other PFCs.⁴¹ Only J-coupled T₂ values were measured for the CF₂ multiplet at 3 T, since the RF bandwidth could not be decreased to selectively excite the CF and CF₂ peaks. The true J-coupled T₂ relaxation times might be even shorter than what we were able to measure with the relatively slow spin echo sequence; overall this would make these resonances rather unsuitable for MRI. It should also be noted that residual small stimulated echo contributions might cause the T₂ values to be slightly overestimated at 3T due to the use of constant spoiler gradients in the CPMG multi-echo spin echo pulse sequence.

Colotti et al. investigated the difference in relaxation times between various in vitro and ex vivo PFPE samples, and observed a mild influence (≤13%) of the difference in relaxation times on the acquisition efficiency.³⁰ We expect that ABL-101 would demonstrate similarly mild differences in relaxation times in

various in vitro and ex vivo conditions. Furthermore, no in vivo relaxation times were measured in this study, because an unlocalized measurement would result in a mix of many tissue compartments with different conditions, while mapping the relaxation times with acceptable precision would most likely take too long. Measuring these could be of interest for future studies though.

Given that the relaxation times of ABL-101 at 3 T are very similar to those of the CF₃ resonance of PFOB, the optimized pulse sequence parameters are also very similar.³⁹ The detection limits of the various optimized pulse sequences were fairly comparable, with a performance loss for all at 37°C compared to at 24°C, most likely due to the longer T₁ relaxation time. This was also observed in the detection limit calculations by Colotti et al.³⁹ Furthermore, since the same MR scanner, RF coil and temperature as well as a similarly optimized TSE and bSSFP pulse sequences were used in those detection limit calculations, these values can be directly compared, and the detection limit of ABL-101 is lower than that of other investigated PFCs (PFPE, PFCE and PFOB) with all pulse sequences at the exception of the detection limit of the PFCE determined with the bSSFP pulse sequence. Our optimization techniques and predicted optima agreed also well with those suggested in prior studies by Faber et al.⁴² and Constantinides et al.,⁴³ but since we use different RF coils and magnetic field strengths, the sensitivities or SNR levels cannot be compared between the studies.

When translating the optimized imaging parameters to the clinical setting, certain parameter combinations together with specific RF coils and body parts might lead to SAR constraints, in which case parameters might need to be adapted and a slightly reduced SNR efficiency will be obtained.

The imaging experiment of the syringes with the anesthetic isoflurane and ABL-101 demonstrated that no isoflurane could be detected when acquiring images at the ABL-101 CF₃ frequency and vice versa. This was confirmed in the in vivo study, where the isoflurane did not generate confounding signals in the subcutaneous fat of the mice.

The longitudinal data acquired from the three mice administered with ABL-101 suggests a clearance half-life in the spleen of 6.85 ± 0.45 days at a dose of 3 ml/kg. This tissue clearance is shorter than those determined with MRI for other PFCs such as PFCE, PFOB, and PFD, (250 days, 12 days, and 9 days, respectively).⁴⁰ Although this encouraging result might be due to the lower injected dose in our study (since prior studies for PFOB with lower doses found similar clearance half-lives of 3 to 8 days),^{3,44} this low injected quantity is the upper dose used in clinical trials, and indicates that clearance at lower doses might even be faster.

There are several limitations to this study. A low number of animals was used in the clearance substudy, and the clearance of only one dose was described. A smaller ABL-101 dose was in fact tried, but it mostly failed due to the low precision of the tail vein injections. The reported relatively broad particle size distribution in the emulsion might cause the emulsion to be taken up by a range of cell types, and might impact the specificity for inflammation imaging and cell tracking. However, it should be noted that in past clinical trials, the emulsion was homogenized with a mixing procedure prior to intravenous clinical use. Finally the ¹⁹F relaxation times of PFCs are also known to be affected by the oxygen tension, to point that the relaxation times can be used for non-invasive measurement of oxygen tension.^{45,46} However, we did not assess this influence in this study, and it might thus be an interesting subject for future studies, especially given that ABL-101 is being assessed for improved oxygen delivery in clinical trials.

In conclusion, the characteristics of ABL-101 as a ¹⁹F MRI tracer are similar to those of PFCs developed specifically for MRI, while ABL-101 has a clearance half-life similar to PFCs that have been used in large doses in clinical trials. Overall, ABL-101 appears to be the best of both worlds, and is thus a very promising candidate for future clinical trials that include ¹⁹F MRI for cell tracking or inflammation monitoring.

Acknowledgements

An ABL-101 sample was generously donated by Aurum Biosciences (Glasgow, UK). We would like to thank Aurélien Bornet, PhD and Emilie Baudat, PhD for performing the high-field NMR

experiments, Laurent Lecomte for veterinary assistance with the mouse study, Matthias Stuber, PhD for insightful discussions on the study design, and Katarzyna Pierzchala, PhD for her help with the construction of the ABL-101 phantoms. This study was supported by grants from the Swiss National Science Foundation (PZ00P3_154719 and 32003B_182615).

References

1. Holland GN, Bottomley PA, Hinshaw WS. ^{19}F magnetic resonance imaging. *Journal of Magnetic Resonance (1969)*. 1977;28(1):133-136.
2. Ruiz-Cabello J, Barnett BP, Bottomley PA, Bulte JW. Fluorine (^{19}F) MRS and MRI in biomedicine. *NMR in biomedicine*. 2011;24(2):114-129.
3. Riess JG. Oxygen carriers ("blood substitutes")--raison d'etre, chemistry, and some physiology. *Chem Rev*. 2001;101(9):2797-2920.
4. Temme S, Jacoby C, Ding Z, et al. Technical advance: monitoring the trafficking of neutrophil granulocytes and monocytes during the course of tissue inflammation by noninvasive ^{19}F MRI. *J Leukoc Biol*. 2014;95(4):689-697.
5. Flogel U, Ding Z, Hardung H, et al. In vivo monitoring of inflammation after cardiac and cerebral ischemia by fluorine magnetic resonance imaging. *Circulation*. 2008;118(2):140-148.
6. Kadayakkara DK, Ranganathan S, Young WB, Ahrens ET. Assaying macrophage activity in a murine model of inflammatory bowel disease using fluorine-19 MRI. *Lab Invest*. 2012;92(4):636-645.
7. van Heeswijk RB, De Blois J, Kania G, et al. Selective in vivo visualization of immune-cell infiltration in a mouse model of autoimmune myocarditis by fluorine-19 cardiac magnetic resonance. *Circ Cardiovasc Imaging*. 2013;6(2):277-284.

8. Shin SH, Park SH, Kim SW, Kim M, Kim D. Fluorine MR Imaging Monitoring of Tumor Inflammation after High-Intensity Focused Ultrasound Ablation. *Radiology*. 2018;287(2):476-484.
9. van Heeswijk RB, Pellegrin M, Fogel U, et al. Fluorine MR Imaging of Inflammation in Atherosclerotic Plaque in Vivo. *Radiology*. 2015;275(2):421-429.
10. Waiczies H, Lepore S, Drechsler S, et al. Visualizing brain inflammation with a shingled-leg radio-frequency head probe for $^{19}\text{F}/^1\text{H}$ MRI. *Sci Rep*. 2013;3:1280.
11. Gaudet JM, Ribot EJ, Chen Y, Gilbert KM, Foster PJ. Tracking the fate of stem cell implants with fluorine-19 MRI. *PLoS One*. 2015;10(3):e0118544.
12. Srinivas M, Boehm-Sturm P, Figdor CG, de Vries IJ, Hoehn M. Labeling cells for in vivo tracking using (^{19}F) MRI. *Biomaterials*. 2012;33(34):8830-8840.
13. Ahrens ET, Helfer BM, O'Hanlon CF, Schirda C. Clinical cell therapy imaging using a perfluorocarbon tracer and fluorine-19 MRI. *Magnetic resonance in medicine*. 2014;72(6):1696-1701.
14. Mastropietro A, De Bernardi E, Breschi GL, et al. Optimization of rapid acquisition with relaxation enhancement (RARE) pulse sequence parameters for (^{19}F) -MRI studies. *Journal of magnetic resonance imaging : JMRI*. 2014;40(1):162-170.
15. Liang S, Dresselaers T, Louchami K, Zhu C, Liu Y, Himmelreich U. Comparison of different compressed sensing algorithms for low SNR ^{19}F MRI applications-Imaging of transplanted pancreatic islets and cells labeled with perfluorocarbons. *NMR in biomedicine*. 2017;30(11).
16. Bonner F, Merx MW, Klingel K, et al. Monocyte imaging after myocardial infarction with ^{19}F MRI at 3 T: a pilot study in explanted porcine hearts. *European heart journal cardiovascular Imaging*. 2015;16(6):612-620.

17. van Heeswijk RB, Colotti R, Darcot E, et al. Chemical shift encoding (CSE) for sensitive fluorine-19 MRI of perfluorocarbons with complex spectra. *Magnetic resonance in medicine*. 2018;79(5):2724-2730.
18. Giraudeau C, Flament J, Marty B, et al. A new paradigm for high-sensitivity 19F magnetic resonance imaging of perfluorooctylbromide. *Magnetic resonance in medicine*. 2010;63(4):1119-1124.
19. Tirota I, Mastropietro A, Cordiglieri C, et al. A superfluorinated molecular probe for highly sensitive in vivo (19)F-MRI. *J Am Chem Soc*. 2014;136(24):8524-8527.
20. Deuchar GA, Brennan D, Holmes WM, Shaw M, Macrae IM, Santosh C. Perfluorocarbon Enhanced Glasgow Oxygen Level Dependent (GOLD) Magnetic Resonance Metabolic Imaging Identifies the Penumbra Following Acute Ischemic Stroke. *Theranostics*. 2018;8(6):1706-1722.
21. Deuchar GA, van Kralingen JC, Work LM, et al. Preclinical Validation of the Therapeutic Potential of Glasgow Oxygen Level Dependent (GOLD) Technology: a Theranostic for Acute Stroke. *Transl Stroke Res*. 2018;In Press.
22. Arnaud F, Sanders K, Sieckmann D, Moon-Massat P. In vitro alteration of hematological parameters and blood viscosity by the perfluorocarbon: Oxycyte. *Int J Hematol*. 2016;103(5):584-591.
23. Zhou Z, Sun D, Levasseur JE, et al. Perfluorocarbon emulsions improve cognitive recovery after lateral fluid percussion brain injury in rats. *Neurosurgery*. 2008;63(4):799-806; discussion 806-797.
24. Haque A, Scultetus AH, Arnaud F, et al. The Emulsified PFC Oxycyte((R)) Improved Oxygen Content and Lung Injury Score in a Swine Model of Oleic Acid Lung Injury (OALI). *Lung*. 2016;194(6):945-957.

25. Torres LN, Spiess BD, Torres Filho IP. Effects of perfluorocarbon emulsions on microvascular blood flow and oxygen transport in a model of severe arterial gas embolism. *J Surg Res.* 2014;187(1):324-333.
26. Tenax Therapeutics Inc. NCT00908063 - Safety and Tolerability of Oxycyte in Patients With Traumatic Brain Injury (TBI) (STOP-TBI). Nov 13, 2014. Available at: <https://clinicaltrials.gov/ct2/show/NCT00908063>. Accessed Jan 15, 2019.
27. Tenax Therapeutics Inc. NCT00174980 - Study of Oxycyte in Severe Closed Head Injury. Jun 10, 2011. Available at: <https://clinicaltrials.gov/ct2/show/NCT00174980>. Accessed Jan 15, 2019.
28. NHS Greater Glasgow and Clyde. NCT03463551 - Perfluorocarbon (ABL-101) Oxygenation for Stroke: Trial With GOLD (Glasgow Oxygen Level Dependent Technology) Imaging Theranostic (POST-IT). Aug 2, 2018. Available at: <https://clinicaltrials.gov/ct2/show/NCT03463551>. Accessed Jan 15, 2019.
29. Poon CS, Henkelman RM. Practical T2 quantitation for clinical applications. *Journal of magnetic resonance imaging : JMRI.* 1992;2(5):541-553.
30. Colotti R, Bastiaansen JAM, Wilson A, et al. Characterization of perfluorocarbon relaxation times and their influence on the optimization of fluorine-19 MRI at 3 tesla. *Magnetic resonance in medicine.* 2017;77(6):2263-2271.
31. Scheffler K, Lehnhardt S. Principles and applications of balanced SSFP techniques. *Eur Radiol.* 2003;13(11):2409-2418.
32. Watts R, Wang Y. k-space interpretation of the Rose Model: noise limitation on the detectable resolution in MRI. *Magnetic resonance in medicine.* 2002;48(3):550-554.
33. Constantinides C, Maguire ML, Stork L, et al. Temporal accumulation and localization of isoflurane in the C57BL/6 mouse and assessment of its potential contamination in (19) F

- MRI with perfluoro-crown-ether-labeled cardiac progenitor cells at 9.4 Tesla. *Journal of magnetic resonance imaging : JMRI*. 2017;45(6):1659-1667.
34. van Heeswijk RB, Pilloud Y, Flogel U, Schwitter J, Stuber M. Fluorine-19 magnetic resonance angiography of the mouse. *PLoS One*. 2012;7(7):e42236.
 35. Woglom WH. The Size of the Spleen in Immune Mice. *The Journal of Cancer Research*. 1919;4(3):281-323.
 36. Melloul E, Raptis DA, Boss A, et al. Small animal magnetic resonance imaging: an efficient tool to assess liver volume and intrahepatic vascular anatomy. *J Surg Res*. 2014;187(2):458-465.
 37. Goette MJ, Keupp J, Rahmer J, Lanza GM, Wickline SA, Caruthers SD. Balanced UTE-SSFP for ¹⁹F MR imaging of complex spectra. *Magnetic resonance in medicine*. 2015;74(2):537-543.
 38. Jacoby C, Oerther T, Temme S, Schrader J, Floegel U. Simultaneous MR Imaging at Different Resonance Frequencies Using Multi Chemical Shift Selective (MCSS) RARE. Paper presented at: 22nd Annual Meeting of ISMRM2014; Milan, Italy.
 39. Colotti R, Bastiaansen JA, Wilson A, et al. Characterization of perfluorocarbon relaxation times and their influence on the optimization of fluorine-19 MRI at 3 tesla. *Magnetic resonance in medicine*. 2016.
 40. Jacoby C, Temme S, Mayenfels F, et al. Probing different perfluorocarbons for in vivo inflammation imaging by ¹⁹F MRI: image reconstruction, biological half-lives and sensitivity. *NMR in biomedicine*. 2014;27(3):261-271.
 41. Kadayakkara DK, Damodaran K, Hitchens TK, Bulte JW, Ahrens ET. (¹⁹F) spin-lattice relaxation of perfluoropolyethers: Dependence on temperature and magnetic field strength (7.0-14.1T). *Journal of magnetic resonance*. 2014;242:18-22.

42. Faber C, Schmid F. Pulse Sequence Considerations and Schemes. In: *Fluorine magnetic resonance imaging*. Pan Stanford Publishing; 2016:1-28.
43. Constantinides C, Maguire M, McNeill E, et al. Fast, quantitative, murine cardiac ^{19}F MRI/MRS of PFCE-labeled progenitor stem cells and macrophages at 9.4T. *PLoS One*. 2018;13(1):e0190558.
44. Mitten RM, Burgan AR, Hamblin A, et al. Dose Related Biodistribution & Elimination of 100% PFOB Emulsion. *Biomaterials, Artificial Cells and Artificial Organs*. 1988;16(1-3):683-684.
45. Mason RP, Antich PP, Babcock EE, Constantinescu A, Peschke P, Hahn EW. Non-invasive determination of tumor oxygen tension and local variation with growth. *Int J Radiat Oncol Biol Phys*. 1994;29(1):95-103.
46. Zhong J, Sakaki M, Okada H, Ahrens ET. In vivo intracellular oxygen dynamics in murine brain glioma and immunotherapeutic response of cytotoxic T cells observed by fluorine-19 magnetic resonance imaging. *PLoS One*. 2013;8(5):e59479.

Tables

Table 1. Fluorine-19 relaxation times of the ABL-101 CF_3 resonance. The T_1 and T_2 relaxation times were measured at temperatures of 24°C and 37°C , and at magnetic field strengths of 3 T, 9.4 T and 14.1 T. Pure ABL-101 had a PFC concentration of 1.2 M (^{19}F concentration 24 M), while the ABL-101-agar mix had a PFC concentration of 0.30M (^{19}F concentration 6.0 M).

	3 T		9.4 T		14.1 T	
Phantom	T_1 [ms]	T_2 [ms]	T_1 [ms]	T_2 [ms]	T_1 [ms]	T_2 [ms]

24°C						
ABL-101-agar mix	1098 ± 48	344 ± 2	886 ± 4	121 ± 10	677 ± 10	56 ± 4
ABL-101	900 ± 29	353 ± 7	865 ± 1	149 ± 3	640 ± 15	40 ± 6
37°C						
ABL-101-agar mix	1646 ± 25	443 ± 13	1060 ± 8	147 ± 12	827 ± 15	62 ± 6
ABL-101	1560 ± 19	455 ± 8	1051 ± 4	208 ± 5	791 ± 25	38 ± 4

Table 2. Fluorine-19 relaxation times at the ABL-101 CF-CF₂ resonance frequencies. The T₂ relaxation times were too short to be measured at 9.4 T.

Frequency (ppm)	3 T		9.4 T			
	T ₁ [ms]	T ₂ [ms]	T ₁ [ms]	T ₁ [ms]	T ₁ [ms]	
	-115	-115	-125	-138	-144	
24°C						
ABL-101-agar mix	1091 ± 22	4.6 ± 1.6	914 ± 9	865 ± 10	816 ± 15	1220 ± 60
ABL-101	-	-	913 ± 2	873 ± 6	804 ± 6	1045 ± 6
37°C						
ABL-101-agar mix	1715 ± 58	4.2 ± 1.8	1090 ± 13	1035 ± 13	953 ± 13	1210 ± 30
ABL-101	-	-	1116 ± 5	1060 ± 5	983 ± 8	1237 ± 10

Table 3. Optimized pulse sequence parameters for ABL-101 at 24°C and 37°C, at 3 T. The optimized parameters of the TSE pulse sequence were calculated for BW = 130Hz/px and TE = 13 ms for the CF₃ resonance and BW = 250 Hz/px and TE = 8.9 ms for the highest resonance of the CF-CF₂ groups. LMR = longitudinal magnetization restoration. The optimized flip angles of the bSSFP pulse sequence were calculated with the relaxation times of pure ABL-101.

Frequency	TSE (LMR off)		TSE (LMR on)		bSSFP
	TR [ms]	ETL	TR [ms]	ETL (-)	flip angle (°)
24°C					
CF ₃	1777	26	800	12	64
CF-CF ₂ group	1370	1	1380	1	7
37°C					
CF ₃	2857	35	1180	15	57
CF-CF ₂ group	2150	1	2150	1	6

Table 4. Detection limits of ABL-101 with three pulse sequences. The detection limit indicates the concentration that will result in SNR=4 at the acquired voxel size of 0.25mm³ and the respective acquisition duration. These concentrations are then normalized to the ¹⁹F atom content per PFC molecule, an acquisition duration of 10min, and a voxel size of 1mm³, as per Colotti et al.³⁰

	Temperature (°C)	TSE (LMR off)	TSE (LMR on)	bSSFP
PFC detection limit (mM)	24	5.88	6.44	11.6
	37	7.21	7.75	14.5
Acquisition time		203 s	211 s	51.6 s
Normalized ¹⁹ F detection limit (mM)	24	17.1	19.2	17.0
	37	21.3	23.1	21.3

Figures

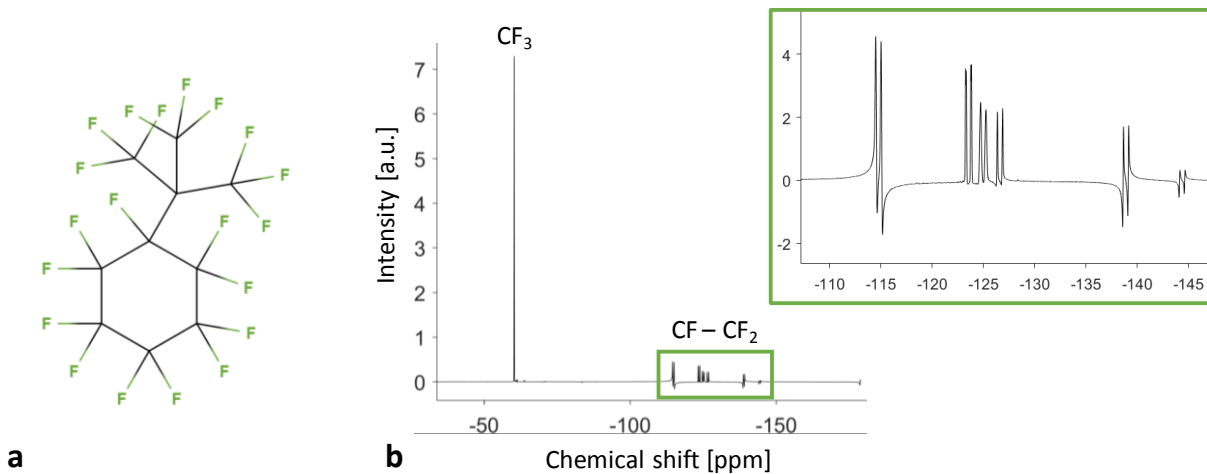


Figure 1. ABL-101 perfluorocarbon structure and spectrum. **a.** Perfluoro(t-butyl)cyclohexane, the perfluorocarbon in ABL-101, is composed of 5 CF₂ groups, 1 CF group and 3 CF₃ groups. **b.** The ABL-101 spectrum consists of a large singlet that corresponds to the CF₃ groups, and a multiplet of several smaller resonances (inset) that corresponds to the J-coupled CF-CF₂ groups. This spectrum was obtained at 14.1 T with the resonance frequency of trifluoroacetic acid (TFA) set to 0 ppm.

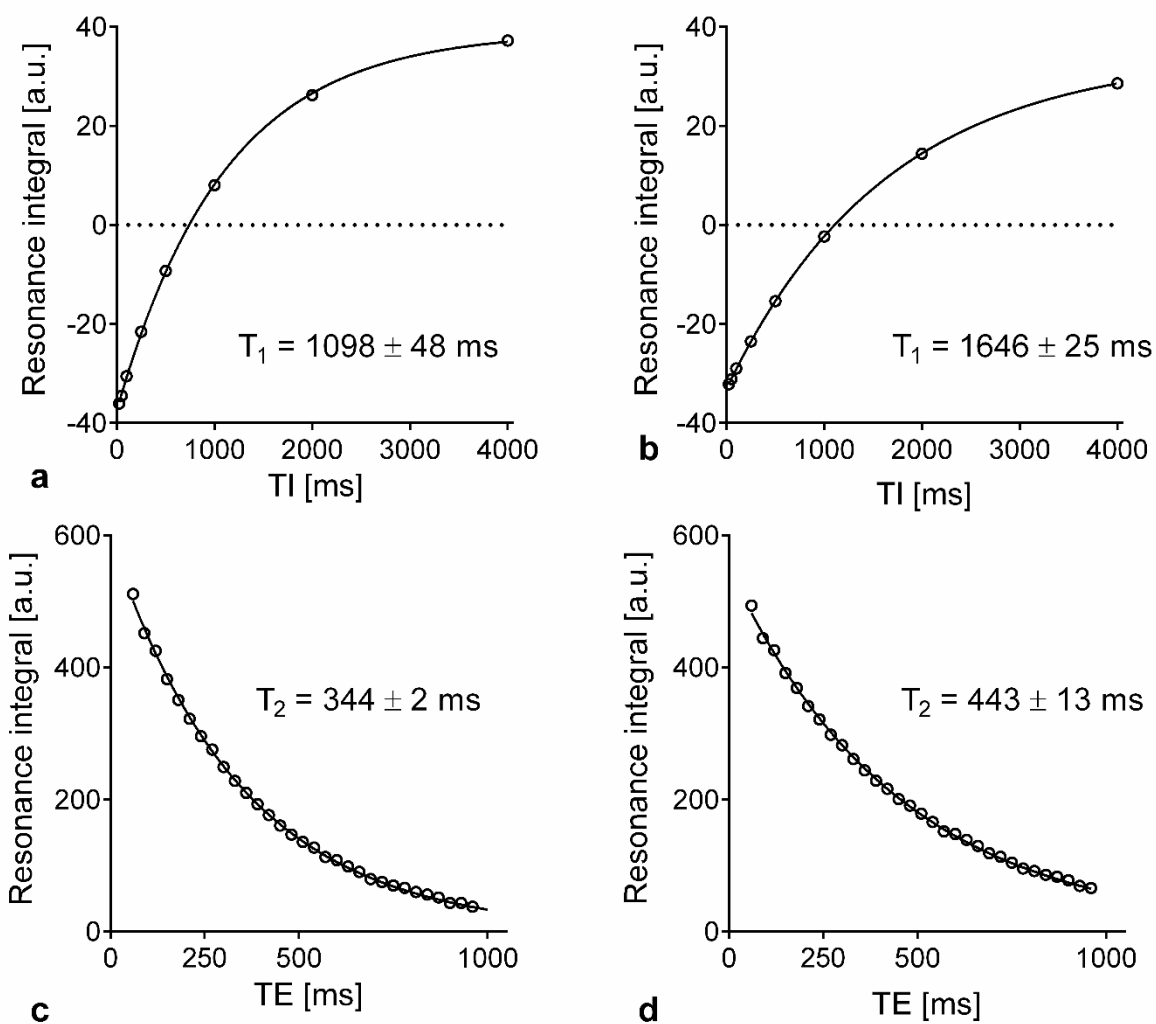


Figure 2. Representative T₁ and T₂ relaxations of the ABL-101 CF₃ resonance in an agar gel. a. The T₁ relaxation and its curve fit at 3T and 24°C. **b.** The T₁ relaxation and its curve fit at 3T and 37°C. **c.** The T₂ relaxation and its curve fit at 3T and 24°C. **d.** The T₂ relaxation and its curve fit at 3T and 37°C. All relaxation curves could be fitted precisely with their model, and resulted in $R^2 \geq 0.999$. The first echo of both T₂ relaxation curves was not used since it lacks the minor contribution of stimulated echoes of the later points, and would skew the T₂ fit.

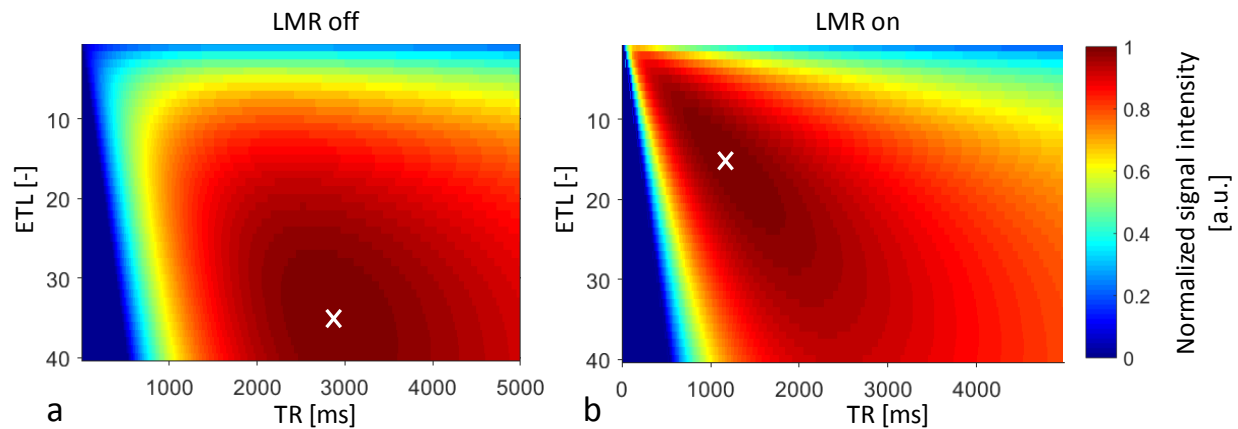


Figure 3. TSE parameter optimization for the pure ABL-101 CF_3 resonance at 3 T and 37°C . Maps of the normalized signal intensity with the longitudinal magnetization restoration (LMR) **a.** off and **b.** on. The optimized parameters were ETL = 35, TR = 2857 ms for LMR off and ETL = 15, TR = 1180 ms for LMR on, with BW = 130 Hz/px and TE = 13 ms for both simulations (white crosses). Both optima are relatively broad and require large parameter changes for an effect on the acquisition efficiency.

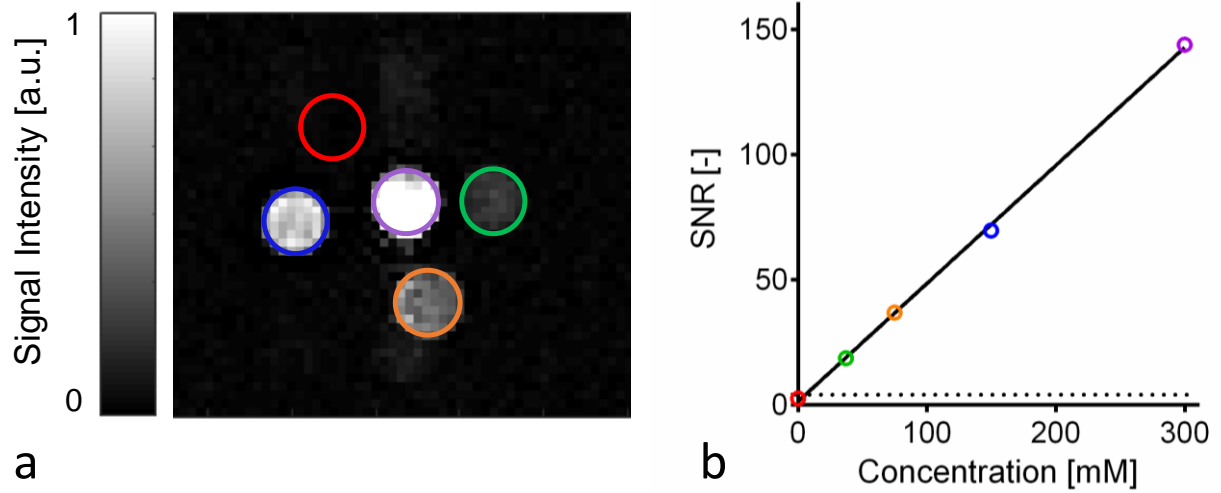


Figure 4. Detection limit of ABL-101 at 3 T. **a.** ^{19}F image of the ABL-101 phantom: four tubes are visible; the red ROI of the fifth tube without ABL-101 only contains noise. **b.** Fit of the SNR in the tubes as a function of the corresponding ABL-101 concentration. The dotted line indicates the Rose criterion, below which signal can be confused with noise ($\text{SNR} = 4$). A linear fit (solid line) provided a detection limit of 5.88 mM of ABL-101 for an acquisition time of 203 seconds at 24°C.

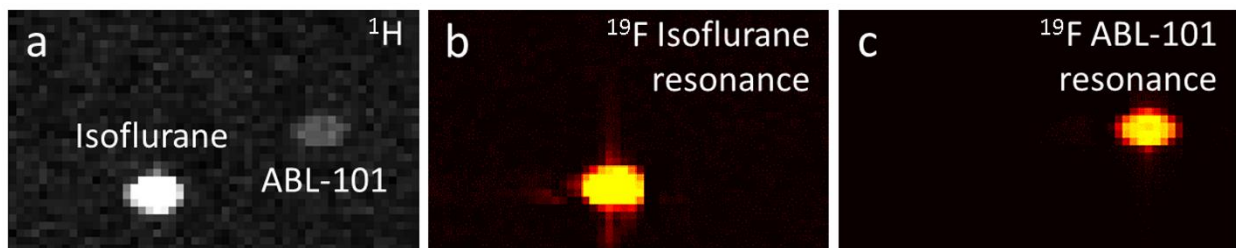


Figure 5. A demonstration of the sufficiently large spectral separation between the isoflurane and ABL-101 resonances. a. A ^1H reference image through a tube with isoflurane and a tube with ABL-101. **b.** A ^{19}F TSE image with the resonance frequency set to the isoflurane peak closest to that of ABL-101. The isoflurane tube is visible, while the ABL-101 tube is not. **c.** When the ABL-101 resonance frequency is used, the visibilities are switched and only the ABL-101 tube is visible.

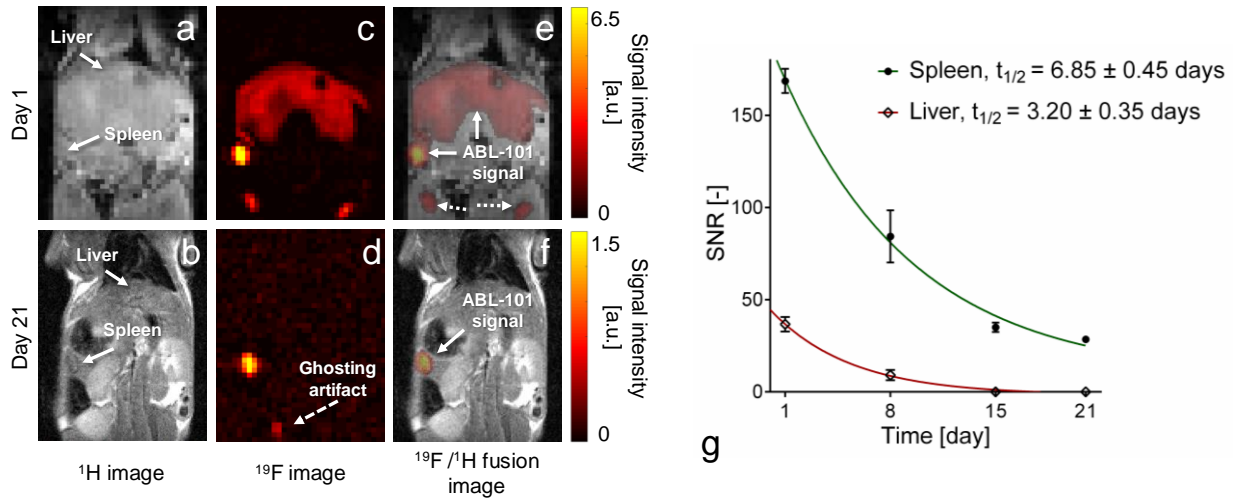


Figure 6. Detection of ABL-101 signal in mouse liver and spleen at 3 T and related clearance half-lives. a, b. ^1H images of the mouse anatomy, **c, d.** ^{19}F images and **e, f.** fusion of the ^1H and ^{19}F images, one and 21 days after injection respectively. One day after injection, the ^{19}F signal is visible in both the spleen and liver (white arrows). Signal was also observed in potential lymph nodes (dotted arrows). Twenty-one days after injection, the ^{19}F signal is visible in the spleen only and was completely cleared from the liver. A small ghosting artifact that continues in adjacent slices and that bled out from the very strong signal of the reference tube can be observed in the ^{19}F image (dashed arrow). **g.** SNR measurements from day one to day 21 after ABL-101 injection ($n = 3$ animals, ABL-101 dosage = 3 mL/kg). The clearance from the liver was extremely fast since no ^{19}F signal was observed after 15 days.